# Analysis of resolution for an amplitude-steered array

Catherine H. Frazier[a)]
*Bioacoustics Research Laboratory, Department of Electrical and Computer Engineering, University of Illinois at Urbana-Champaign, Urbana, Illinois 61801*

W. Jack Hughes[b)]
*Applied Research Laboratory, The Pennsylvania State University, P.O. Box 30, State College, Pennsylvania 16801*

William D. O'Brien, Jr.[c)]
*Bioacoustics Research Laboratory, Department of Electrical and Computer Engineering, University of Illinois at Urbana-Champaign, Urbana, Illinois 61801*

(Received 10 June 1999; accepted for publication 16 February 2000)

In 1976, Hughes and Thompson introduced the idea of steering the maximum response of a linear array by amplitude weighting the output signals of the elements, thus eliminating the need for time delays or phase-shift networks. Currently that amplitude-steered array concept is being extended to a broadband two-dimensional array that can be used for real-time three-dimensional imaging. In shifting the use of the amplitude-steered array from underwater acoustic communications to imaging, we must consider different issues of the array's performance such as lateral and axial resolution. For the linear amplitude-steered array, we show that both lateral and axial resolution are limited by the length of the array. The dependence of axial resolution on the length of the array is a unique feature of the amplitude-steered array, leading to an interesting tradeoff between lateral and axial resolution. A theoretical basis for the dependence is developed and simulation results are given.  [S0001-4966(00)03705-X]

PACS numbers: 43.30.Yj, 43.30.Wi [DLB]

## INTRODUCTION

The concept of steering an array using amplitude weighting was introduced by Hughes and Thompson in 1976.[1] Although amplitude weighting is essentially an apodization, in this discussion the desired effect is to steer the main lobe, not to lower sidelobes. The intent of amplitude steering is to tilt the maximum response of the beam pattern without using multiple delay lines or phase-shift networks, which are bulky. Amplitude weighting is implemented passively, using fixed weights, in order to achieve this advantage in terms of cost and complexity.

In the original formulation of the amplitude-steered array, the beam was steered to a particular direction at a single frequency, and the fact that the steering direction changed with frequency was considered a drawback of the design. In this study, we use the change in steering direction with frequency to design a fast imaging system. By exciting the array with an impulsive or broadband linear frequency modulated (FM) chirp signal, the maximum array response is swept over a range of angles. A sector is scanned using a single broadband transmit pulse, leading to fast two-dimensional imaging of the sector, compared to conventional imaging that uses one transmit pulse for each steering direction. Even more exciting than two-dimensional imaging is the potential expansion to real-time three-dimensional imaging, which is currently being developed.

[a)]Electronic mail: hillsley@uiuc.edu
[b)]Electronic mail: wjh2@psu.edu
[c)]Electronic mail: wdo@uiuc.edu

Figure 1 is a diagram of the imaging geometry. The steering direction of the main beam is defined by the angle $\theta$ measured from the array broadside direction. The axial and lateral directions are defined with reference to the steering direction. The axial direction is along the steering direction, and the lateral direction is perpendicular to it. A linear FM chirp with defined start and stop frequencies would sweep the main lobe over the sector defined in the figure by angled solid black lines.

Axial resolution is defined as the spatial length of the received pulse. The amplitude-steered array operated in broadband mode possesses a unique quality that axial resolution is dependent on the length of the array. In traditional imaging with an array of equiamplitude elements, where the transducer is shock-excited, axial resolution is independent of the length of the array, but dependent on the wavelength at the resonance frequency and on the $Q$ of the transducer, where $Q$ is defined as $2\pi$ times the energy stored at resonance divided by the energy dissipated per cycle.[2] For the amplitude-steered array, resolution in the lateral direction can be traded for resolution in the axial direction by changing the array length. It is the unique relationship between axial and lateral resolution of the amplitude-steered array that is explored in this paper.

Section I gives a brief overview of amplitude steering and image formation using this array. We recommend that readers refer to Ref. 1 for a more complete discussion of amplitude steering. Section II defines axial and lateral resolution for the purpose of this paper. Section III describes the tradeoff between axial and lateral resolution. In Sec. IV,

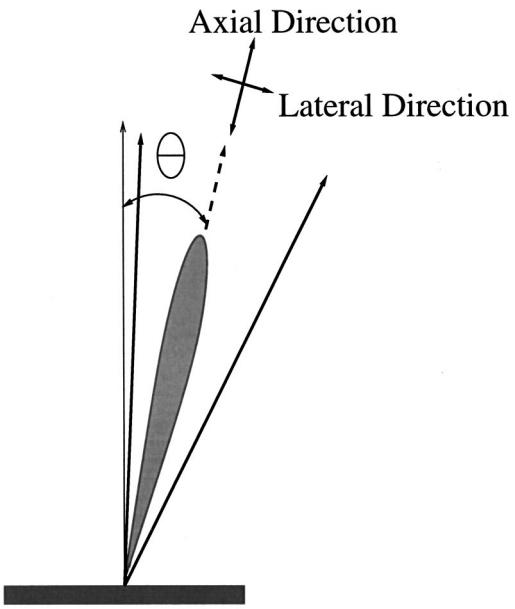


FIG. 1. Description of the imaging scenario. The steering direction of the main beam is given by the angle $\theta$. Axial and lateral directions are defined relative to the steering direction.

simulation results are presented. And in Sec. V, conclusions are given.

## I. AMPLITUDE STEERING AND IMAGE FORMATION

We will use the amplitude-steered array in pulse-echo mode, so each of the elements is both a transmitter and a receiver. In this discussion, we first consider the one-way far-field pressure of a linear array of equally spaced, equiamplitude point sources. To steer the main lobe to $\theta_0$, the signal from each element can be phase-shifted by multiplying by the factor $e^{-j(nk_0d\sin\theta_0)}$, where $n$ is an index used to enumerate the elements, $k_0$ is the wave number at a particular frequency, and $d$ is the distance between the elements. This phase shift will only steer the main lobe to $\theta_0$ at the frequency used to calculate $k_0$; therefore, a fixed phase shift is generally used for narrow-band operation. The pressure field can be expressed as

$$P(r,\theta)=\frac{e^{-jkr}}{r}\sum_n e^{jnd(k\sin\theta-k_0\sin\theta_0)}=\frac{Ne^{-jkr}}{r}H(\theta). \tag{1}$$

Now, we consider only the array pattern, $H(\theta)$. We assume that we have an array with an even number of elements, $N$, and we measure the phase for each element relative to the center of the array. To simplify the expression, we replace $(kd/2)\sin\theta$ with $u$ and $(k_0d/2)\sin\theta_0$ with $\phi$.

$$H(\theta)=\frac{1}{N}\sum_{n=-N/2+1}^{N/2} e^{j(2n-1)(u-\phi)}. \tag{2}$$

Combining terms of the sum in pairs, we have

$$H(\theta)=\frac{2}{N}[\cos(u-\phi)+\cos(3(u-\phi))+\ldots +\cos((N-1)(u-\phi))]. \tag{3}$$

Using the trigonometric identity for the cosine of a sum, Eq. (3) can be rewritten as

$$H(\theta)=\frac{2}{N}[\cos\phi\cos u+\cos 3\phi\cos 3u+\ldots +\cos((N-1)\phi)\cos((N-1)u)+\sin\phi\sin u +\sin 3\phi\sin 3u+\ldots+\sin((N-1)\phi)\sin((N-1)u)]. \tag{4}$$

A corresponding equation for an array with an odd number of elements is

$$H(\theta)=\frac{2}{N}[0.5+\cos 2\phi\cos 2u+\cos 4\phi\cos 4u+\ldots +\cos((N-1)\phi)\cos((N-1)u)+\sin 2\phi\sin 2u +\sin 4\phi\sin 4u+\ldots+\sin((N-1)\phi)\sin((N-1)u)]. \tag{5}$$

Using Eq. (4), we shift our interpretation of how the beam steering is achieved. At the beginning of this discussion, we steered the beam by phase-shifting a linear array of equiamplitude elements. Now we steer the beam by weighting the elements. In Eq. (4), $\cos((2n-1)\phi)$ and $\sin((2n-1)\phi)$ terms are constants which we interpret as amplitude weights on the elements. The $\cos((2n-1)u)$ and $\sin((2n-1)u)$ terms represent combinations of pairs of elements on opposite sides of the center of the array in phase or 180° out of phase. Therefore, Eq. (4) can be interpreted as the sum of the outputs of two arrays. The first array [sum of $\cos(2n-1)u$ terms] combines elements on opposite sides of the center with equal amplitudes and in phase. We call this the phase-symmetric array. The second array [sum of $\sin(2n-1)u$ terms] combines elements on opposite sides of the array with equal amplitudes and 180° out of phase. We call this the phase-antisymmetric array. According to the equation, the outputs of the two arrays should be added in phase; however, the output of a phase-antisymmetric array is inherently 90° out of phase with the output of a phase-symmetric array. The outputs of the two arrays, therefore, must be added with an additional $\pm 90°$ shift.[3] The sign of the shift determines whether the beam is tilted toward positive $\theta_0$ or toward negative $\theta_0$. Conceptually, we have used two arrays or one array with two sets of weights to achieve beamsteering. In practice, the array layout is designed such that the phase-symmetric and phase-antisymmetric arrays share the same space. The $\cos(2n-1)\phi$ and $\sin(2n-1)\phi$ factors in Eq. (4) are the amplitude weights which determine the steering direction of the main beam, but they do not have any effect on sidelobe levels. Further apodization can be applied to achieve reduced sidelobe levels.

If the array described above is excited by a frequency different from the design frequency used to calculate $\phi$, the maximum response will occur at an angle different from the designed steering direction, $\theta_0$.

$$\phi=\frac{k_0d}{2}\sin\theta_0=\frac{k_fd}{2}\sin\theta_f. \tag{6}$$

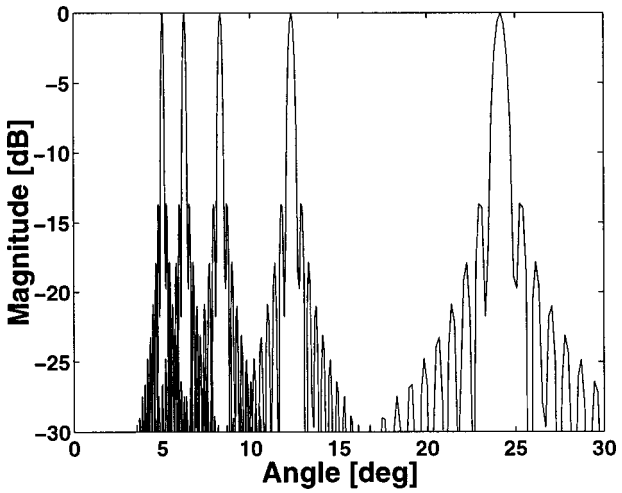


FIG. 2. Beams from a 9.76-cm-length aperture steered to 5° at 5.6 MHz. Beams are shown for 5.6 MHz (5°), 4.5 MHz (6.23°), 3.4 MHz (8.25°), 2.3 MHz (12.25°), and 1.2 MHz (24°).

The subscript, $f$, was added to $k$ and $\theta$ to emphasize that the new steering direction is calculated for a specific frequency, $f$. Rearranging to solve for the new steering direction, $\theta_f$, gives

$$\theta_f = \sin^{-1}\left(\frac{k_0}{k_f}\sin\theta_0\right), \tag{7}$$

which can be restated as

$$\theta_f = \sin^{-1}\left(\frac{f_0}{f}\sin\theta_0\right). \tag{8}$$

As the frequency increases, the angle that the beam is steered away from broadside decreases. An example of several beams from one array is shown in Fig. 2. The 9.76-cm-length array is designed to steer to 5° at 5.6 MHz. Beams are shown for 5.6 MHz (5°), 4.5 MHz (6.23°), 3.4 MHz (8.25°), 2.3 MHz (12.25°), and 1.2 MHz (24°). Note that as the frequency decreases, the beamwidths increase and the spacing between the beams also increases.

In Fig. 2, we have shown a discrete set of beams. By transmitting a linear FM chirp, the beam is swept continuously over a sector as the frequency changes. The array, operated in pulse-echo mode, transmits a pulse and receives the echo. The output of the array is a single radio frequency (rf) signal from which the image is made. To form a two-dimensional image, the received signal is first filtered with a matched filter for pulse-compression. Then the short-time Fourier transform (STFT) is calculated. The position of the fast Fourier transform (FFT) window gives range information, and the frequencies contained in the window give lateral position information. The image is the spectrogram, which is the magnitude squared of the STFT.

## II. DEFINITION OF RESOLUTION

We will use one-point definitions for lateral and axial resolution, which correspond to measuring the axial and lateral extent of the point spread function. This definition is used in contrast to a two-point definition, which would specify the minimum separation between two points that allows the points to be distinguished. For the amplitude-steered array of point elements operated at a particular frequency $f$, the array pattern can be written as

$$H(\theta) = \frac{1}{N}\frac{\sin((N/2)kd(\sin\theta - \sin\theta_f))}{\sin((1/2)kd(\sin\theta - \sin\theta_f))}. \tag{9}$$

We define lateral resolution as the $-3$-dB width of the one-way array pattern. The $-3$-dB points on either side of the maximum are the points where the argument of the periodic sinc is $\pm 1.3894$. We use the expression

$$\frac{N}{2}kd(\sin\theta_{-3\ \mathrm{dB}} - \sin\theta_f) = \pm 1.3894. \tag{10}$$

Solving for $\theta_{-3\,\mathrm{dB}}$ on each side of the maximum array response,

$$\theta^{+}_{-3\ \mathrm{dB}} = \sin^{-1}\left(\sin\theta_f + \frac{0.4423\lambda}{Nd}\right),$$

$$\theta^{-}_{-3\ \mathrm{dB}} = \sin^{-1}\left(\sin\theta_f - \frac{0.4423\lambda}{Nd}\right),$$

$$\alpha = \theta^{+}_{-3\ \mathrm{dB}} - \theta^{-}_{-3\ \mathrm{dB}}, \tag{11}$$

where $\alpha$ is the lateral resolution in degrees.

Axial resolution is defined as the spatial length of the pulse

$$AR = \frac{ct}{2}, \tag{12}$$

where $c$ is the speed of sound in the medium and $t$ is the temporal length of the pulse. For conventional imaging, where the transducer is shock-excited, this description of axial resolution can be related to an expression for axial resolution which depends on the wavelength at the resonance frequency and on the $Q$ of the transducer, where $Q$ is defined as $2\pi$ times the energy stored at resonance divided by the energy lost per cycle.[2] That expression is given by

$$AR = \frac{Q\lambda}{4}. \tag{13}$$

An alternate definition of $Q$, $Q = f_r/\Delta f$, where $f_r$ is the resonance frequency and $\Delta f$ is measured at half power points, is consistent with the previous definition of $Q$.[4]

We seek a definition of axial resolution that is similar in form to Eq. (13). However, our definition of resolution will not depend on the $Q$ of the transducer, but rather on the inverse of the relative bandwidth of the received signal, $f/\Delta f$ which we call $Q_{\mathrm{sig}}$. We transmit a chirp and then apply matched filtering for pulse compression. The filter operates on the time signal received by the array. The output of the pulse compression operation is approximately a sinc if the time-bandwidth product is large enough,[5]

$$\rho = \frac{\sin(2\pi\Delta f x/c)}{2\pi\Delta f x/c}, \tag{14}$$

where $\rho$ is the correlation between the received signal and the impulse response of the filter, $\Delta f$ is the bandwidth of the received chirp, $c$ is the speed of sound, and $x$ is the range which is calculated as $ct/2$ when the array is operated in

pulse-echo mode. We use the $-3$-dB points of $\rho$ to find the axial resolution. The function falls to $-3$ dB, relative to the maximum, when the argument is equal to $\pm 1.3894$. We write

$$\frac{2\pi f}{c}\frac{\Delta f}{f}x_{-3\ \mathrm{dB}} = 1.3894, \tag{15}$$

and solve for $2x_{-3\ \mathrm{dB}}$, where the factor of 2 accounts for the $-3$-dB points on each side of the maximum. Frequency, $f$, has been multiplied in the numerator and denominator of Eq. (15) so that we may find an expression for axial resolution in terms of wavelength. The expression for axial resolution is

$$AR = 2x_{-3\ \mathrm{dB}} = 0.4423 Q_{\mathrm{sig}}\lambda, \tag{16}$$

where $Q_{\mathrm{sig}}$ is the inverse of the relative bandwidth of the received signal. Although this expression does not explicitly depend on the length of the array, we will see that $Q_{\mathrm{sig}}$ depends on the length through the beamwidth in the next section, where we discuss the tradeoff between axial and lateral resolution. We could have reduced Eq. (15) to an expression for $x_{-3\ \mathrm{dB}}$ that was a function of $\Delta f$; however, we prefer to have an expression in terms of the wavelength so we can see how resolution will change with center frequency, rather than with bandwidth. Note that for good resolution, we would like both $\theta_{-3\ \mathrm{dB}}$ and $x_{-3\ \mathrm{dB}}$ to be small.

Finite element size will change the beamwidth, which affects $Q_{\mathrm{sig}}$ and therefore axial resolution; however, the effect is generally small for practical imaging arrays. For finite elements, the overall array pattern is multiplied by the beam pattern of the individual element, which can narrow the main beam, thus improving the lateral resolution and degrading the axial resolution. The array pattern for the array of point sources is given by Eq. (9). For an array of rectangular elements, the unsteered beam pattern is given by

$$H(\theta) = \frac{1}{N}\frac{\sin\left(\frac{Nkd}{2}\sin\theta\right)}{\sin\left(\frac{kd}{2}\sin\theta\right)}\frac{\sin\left(\frac{ka}{2}\sin\theta\right)}{\frac{ka}{2}\sin\theta}, \tag{17}$$

where $a$ is the width of the element. The largest possible width of the element is the center-to-center spacing of the elements ($a=d$), which would mean that the aperture is continuous. If $N$ is large, the expression for the width of the main beam will be dominated by the periodic sinc term, the array pattern. Likewise, if $a \ll d$, the expression for the width of the main beam will be dominated by the array pattern. In the other extreme, if $a=d$ and $N=2$, the effect of the element size is to double the length of the array compared to the array of two-point elements. In that case and in similar cases where $N$ is small and $a \approx d$, the finite element size will have a larger effect improving lateral resolution and degrading axial resolution.

## III. AXIAL AND LATERAL RESOLUTION TRADEOFF

The amplitude-steered array spatially separates frequencies by virtue of the fixed phase shift used to calculate amplitude weights. If the frequencies could be completely separated, i.e., if the beams were infinitely narrow, a point target within the insonified region would produce a single frequency return, implying that two-point targets separated only in range could not be distinguished. In reality, it is possible to distinguish multiple targets in the same direction at different ranges because beams are not infinitely thin, but overlap due to the finite length of the array.

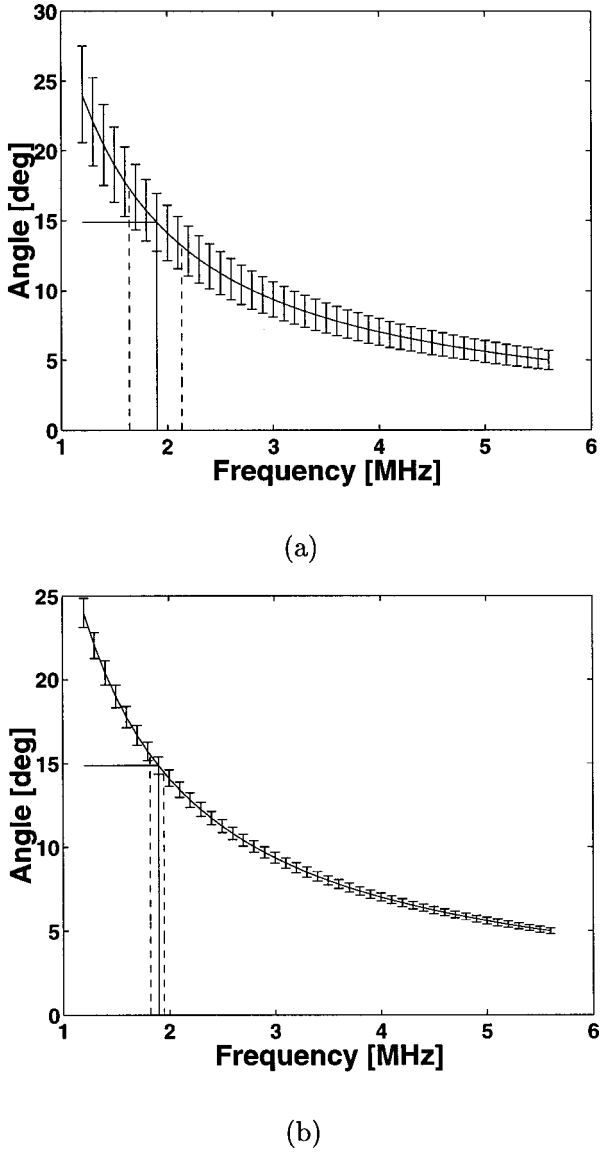


FIG. 3. Lateral and axial resolution for (a) 1-cm-length and (b) 4-cm-length apertures. The line plotted is the steering direction versus frequency. The error bars indicate the $-3$-dB beamwidth at each frequency.

Figure 3 conceptually shows the tradeoff between axial and lateral resolution. In parts (a) and (b), the curve plotted shows the steering direction versus frequency. The error bars indicate the $-3$-dB beamwidth at each frequency. We can see from the error bars that lateral resolution improves with increasing frequency, as expected. Axial resolution can also be determined from these plots. At a particular steering direction, by observing the range of frequencies that overlap, we can determine the bandwidth at that particular direction. In both parts (a) and (b) of Fig. 3, the frequencies that overlap at a steering direction of 15° are located between the dashed lines. The extent of the dashed lines along the frequency axis tells us $\Delta f$. We know the ''resonance fre-

quency,'' the frequency with the greatest amplitude at 15°, from the curve. Therefore, we can determine the wavelength and $Q_{sig}$. Axial resolution, defined by Eq. (16), can be calculated. $Q_{sig}$ is approximately constant over the range of frequencies shown; therefore, axial resolution also improves with increasing frequency.

Figure 3(a) shows field characteristics for a 1-cm-length array. If the length of the aperture is increased from 1 to 4 cm, the lateral resolution improves, illustrated by the decrease in size of the error bars between Fig. 3(a) and (b). However, that decrease in beamwidth implies a decrease in the range of frequencies that overlap in a particular direction, illustrated by the more narrow range between the dashed lines in Fig. 3(a) than in (b). Therefore, $Q_{sig}$ increases with increased array length, and the axial resolution is worsened.

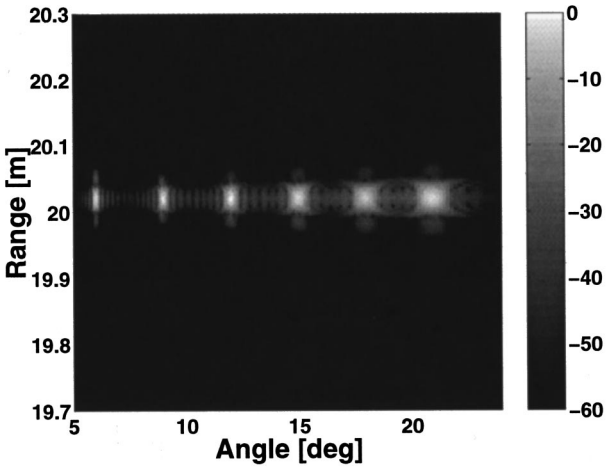


FIG. 4. Image of six simulated targets using 9.76-cm array steered to 5° at 5.6 MHz. The STFT calculation uses a 50.8-$\mu$s Hanning window.

## IV. SIMULATION AND RESULTS

We analyze the tradeoff between axial and lateral resolution for a linear array by simulating the received signal from point targets when the array is used in pulse-echo mode. Three arrays with different lengths are used. The first array has 452 elements with center-to-center spacing of 0.216 mm (9.76-cm-length aperture). For comparison, we also simulate arrays with 694 elements (15-cm-length aperture) and 347 elements (7.5-cm-length aperture), but otherwise similar designs. The amplitude weighting is determined so that the main beam is steered to 5° at 5.6 MHz. The transmitted signal is a linear FM chirp with frequency swept from 1.2 to 5.6 MHz. The targets are placed at 20 m, well beyond the intended maximum range, so that they are in the far field for all steering directions and all array lengths. The angular positions of the targets range from 6 to 24°. The speed of sound is assumed to be 1500 m/s for all simulations. Attenuation is not included. The transducer we simulate has a broadband, low-$Q$ impulse response. The main effect of the transducer's transfer function is to reduce the amplitude of targets away from the resonance frequency of the transducer, not to affect resolution. Therefore, in the simulations we replace the transducer's impulse response with an impulse.

The operation of the linear amplitude steered array has been simulated using the Field II program, developed by J. A. Jensen.[6,7] Figure 4 shows an image of six-point targets imaged using the 452-element array. We can immediately see that both axial and lateral resolution improve with decreasing steering direction, corresponding to increasing frequency.

In order to quantify the tradeoff between axial and lateral resolution, resolutions were measured from images of point targets. In addition to the resolution tradeoff that arises due to the length of the array, there is an additional tradeoff between axial and lateral resolution due to the processing. A STFT is used to form the images. The length of the sliding FFT window affects both lateral and axial resolution of targets. A very short FFT window implies poor frequency resolution and therefore poor lateral resolution, but it also implies good time localization and therefore good axial resolution. The FFT window can be increased to improve lateral resolution until the fundamental limit on lateral resolution due to the length of the array is reached, but a long window means poor axial resolution.

Lateral and axial resolutions were measured from images formed using different length FFT windows in order to reduce the effect of processing on the measurements, so that we could measure the tradeoff in resolution only due to the length of the array. Axial resolution was measured by setting the window length to be short, i.e., 8.333 $\mu$s corresponding to ten cycles of 1.2 MHz. This window length was considered long enough to define a signal at the lowest frequency of the chirp. Lateral resolution was measured by setting the window length to be long, i.e., 0.147 ms. This window length was chosen by increasing the length of the FFT window until the improvement in lateral resolution at 6° was less than 0.5%. The image in Fig. 4 is shown using a window length of 50.8 $\mu$s, which is a compromise between the two extremes.

Measurements were made of the $-3$-dB beamwidths in the lateral direction and the $-3$-dB signal length in the axial direction (Table I). For all steering directions, lateral resolution improves with increasing array length, and axial resolution degrades with increasing array length. Calculated and measured beamwidths and axial resolutions are shown in Figs. 5 and 6, respectively. Calculated beamwidths were

TABLE I. Axial and lateral resolution measurement results.

| Angle (deg) | 6 | 9 | 12 | 15 | 18 | 21 |
|---|---|---|---|---|---|---|
| $f$ (MHz) | 4.669 | 3.120 | 2.347 | 1.886 | 1.579 | 1.362 |
| λ (mm) | 0.321 | 0.481 | 0.639 | 0.795 | 0.950 | 1.10 |
| BW (deg) | | | | | | |
| 7.5 cm | 0.211 | 0.331 | 0.404 | 0.573 | 0.722 | 0.808 |
| 10 cm | 0.174 | 0.254 | 0.316 | 0.440 | 0.539 | 0.613 |
| 15 cm | 0.119 | 0.174 | 0.214 | 0.289 | 0.342 | 0.421 |
| $\Delta f$ (kHz) | | | | | | |
| 7.5 cm | 165 | 110 | 75 | 70 | 60 | 50 |
| 10 cm | 130 | 85 | 60 | 55 | 45 | 40 |
| 15 cm | 95 | 55 | 40 | 35 | 30 | 20 |
| AR (mm) | | | | | | |
| 7.5 cm | 3.845 | 7.690 | 8.972 | 10.25 | 11.54 | 15.38 |
| 10 cm | 6.409 | 8.972 | 11.54 | 12.82 | 15.38 | 17.94 |
| 15 cn | 8.972 | 12.82 | 16.67 | 19.23 | 24.35 | 26.92 |

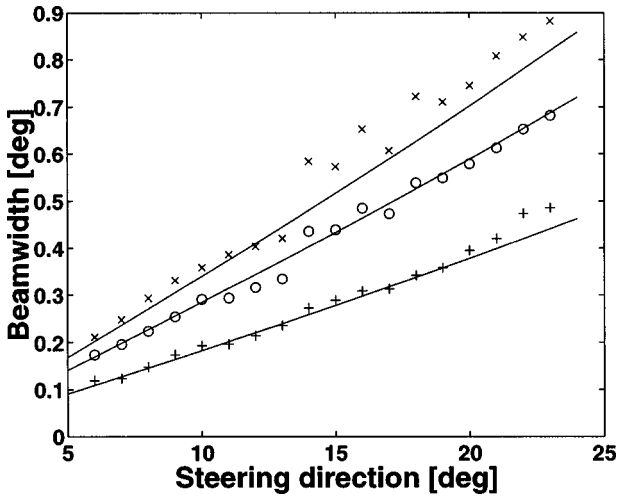


FIG. 5. Comparison of calculated and measured beamwidths. Measured values are given for 7.5-cm length array (×), 9.76-cm length array (○), and 15-cm length array (+). For values measured from simulated images, the STFT calculation uses a 0.147-ms Hanning window. Calculated values are indicated by the solid lines.

found using Eq. (11). Figure 5 shows that beamwidths measured from simulated data agreed with calculated beamwidths to a steering direction of 14°. At higher steering angles, corresponding to lower frequencies, the measured beamwidths were larger than calculated beamwidths. This agreement may be improved by using an even longer FFT window. Axial resolution was calculated using Eq. (16), where $Q_{\text{sig}}$ was calculated using the predicted beamwidths for each frequency and assuming that the array had a flat frequency response. If the steering direction was within the steered $-3$-dB beamwidths of a frequency, $f$, then $f$ was included within $\Delta f$ used to calculate $Q_{\text{sig}}$. Figure 6 shows that the calculated and measured axial resolutions agreed well. The average $Q_{\text{sig}}$ predicted for the 7.5-, 9.76-, and 15-cm apertures are $27.60 \pm 0.094$, $35.90 \pm 0.021$, and $55.18 \pm 0.054$. The average $Q_{\text{sig}}$ measured for the 7.5-, 9.76-, and 15-cm apertures are $28.5 \pm 1.85$, $36.1 \pm 2.01$, and $54.1 \pm 5.45$, respectively.

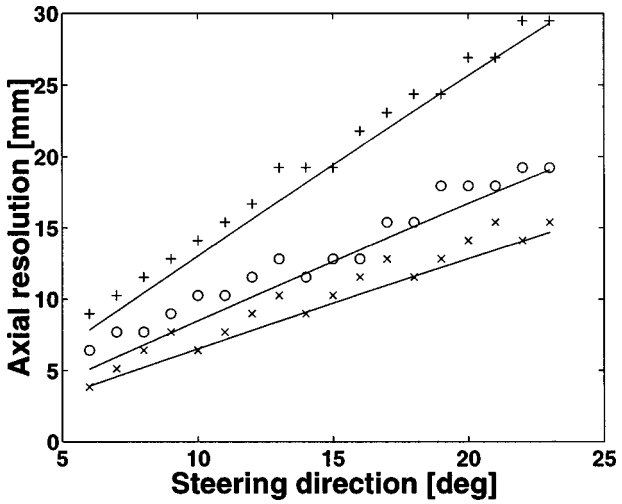


FIG. 6. Comparison of calculated and measured axial resolutions. Measured values are given for 7.5-cm length array (×), 9.76-cm length array (○), and 15-cm length array (+). For values measured from simulated images, the STFT calculation uses an 8.333-$\mu$s Hanning window. Calculated values are indicated by the solid lines.

## V. DISCUSSION AND CONCLUSION

The amplitude-steered array is an array developed to decrease the complexity of electronics used to steer a beam. Amplitude weighting is implemented passively, using fixed weights, so that advantages in terms of cost and complexity over the electronically steered array can be achieved. The array can be used to do fast two-dimensional imaging by exciting it with a broad band of frequencies. When operated with a broadband pulse, the axial resolution is dependent on the length of the array relative to the wavelength, which is different from the operation of conventional transducers.

Fast two-dimensional imaging refers to collecting data for a two-dimensional image with one transmit pulse. The speed of data collection is compared to a conventional, electronically steered array, which transmits at least one pulse per steering direction or line in the image. For each pulse transmitted, the system waits for the pulse to be received from the farthest range of interest before the next pulse is transmitted. In order for the conventional array to collect all the image data with a single transmit pulse, the transmit beam must be broad, so that the entire region of interest is insonified. Then in receive mode, the signals received by the individual elements are stored and used to calculate beams in each of the directions of interest. This imaging method is as fast as ours; however it suffers from a poor signal-to-noise ratio and some loss of resolution because focusing is accomplished only on receive, not on transmit. Other researchers are working on different methods to form orthogonal beams, so that the transmit pattern has multiple main lobes and the targets can be separated with processing.[8]

With the amplitude-steered array, the entire region of interest is insonified by transmitting a broadband pulse. The beams in each direction can be focused by using a focusing lens in front of the array. The signal-to-noise ratio can be improved by lowering the chirp rate, that is, by transmitting a longer signal. Because of the pulse compression, axial resolution is not dependent on the time duration of the pulse, but rather on the bandwidth of the received pulse. The limiting factor in the length of the pulse transmitted is the depth of the ''dead zone,'' the shallow region that cannot be imaged because the transducer is still transmitting; it cannot receive signals.

## ACKNOWLEDGMENTS

This work was supported by DARPA under Contract No. BAA 97-33. The authors would like to thank the anonymous reviewers for their careful review and helpful comments.

[1] W. J. Hughes and W. Thompson, Jr., ''Tilted directional response patterns formed by amplitude weighting and a single 90° phase shift,'' J. Acoust. Soc. Am. **59**, 1040–1045 (1976).
[2] D. A. Christensen, *Ultrasonic Bioinstrumentation* (Wiley, New York, 1988).
[3] E. J. Skudrzyk, *The Foundations of Acoustics* (Springer-Verlag, New York, 1971).

[4] A. D. Pierce, *Acoustics: An Introduction to its Physical Principles and Applications* (Acoustical Society of America, Woodbury, New York, 1991).
[5] D. C. Munson, Jr. and R. L. Visentin, ''A signal processing view of strip-mapping synthetic aperture radar,'' IEEE Trans. Acoust., Speech, Signal Process. **37**(12), 2131–2147 (1989).
[6] Program is available at http://www.it.dtu.dk/~jaj/field/field.html.
[7] J. A. Jensen, ''FIELD: A program for simulating ultrasound systems,'' Med. Biol. Eng. Comput. **34**(1), Suppl. 1, 351–353 (1996).
[8] J. Shen and E. S. Ebbini, ''A new coded-excitation ultrasound imaging system—Part I: Basic principles,'' IEEE Trans. Ultrason. Ferroelectr. Freq. Control **43**(1), 131–140 (1996).